Kodera *et al. Earth, Planets and Space* (2016) 68:202
DOI 10.1186/s40623-016-0567-1

Earth, Planets and Space

FULL PAPER Open Access

Earthquake early warning for the 2016 Kumamoto earthquake: performance evaluation of the current system and the next-generation methods of the Japan Meteorological Agency

Yuki Kodera[1*], Jun Saitou[2], Naoki Hayashimoto[2], Shimpei Adachi[2], Masahiko Morimoto[2], Yuji Nishimae[2] and Mitsuyuki Hoshiba[1]

Abstract

The 2016 Kumamoto earthquake (Kumamoto earthquake sequence) is an extremely high-seismicity event that has been occurring across Kumamoto and Oita Prefectures in Japan since April 14, 2016 (JST). The earthquake early warning system of the Japan Meteorological Agency (JMA) issued warnings for 19 events in the Kumamoto earthquake sequence from April 14 to 19, under some of the heaviest loading conditions since the system began operating in 2007. We analyzed the system performance for cases where a warning was issued and/or strong motion was actually observed. The results indicated that the system exhibited remarkable performance, especially for the most destructive earthquakes in the Kumamoto earthquake sequence. In addition, the system did not miss or seriously under-predict strong motion of any large earthquake from April 14 to 30. However, in four cases, the system issued over-predicted warnings due to the simultaneous occurrence of small earthquakes within a short distance, which implies a fundamental obstacle in trigger-data classifications based solely on arrival time. We also performed simulations using the integrated particle filter (IPF) and propagation of local undamped motion (PLUM) methods, which JMA plans to implement to address over-prediction for multiple simultaneous earthquakes and under-prediction for massive earthquakes with large rupture zones. The simulation results of the IPF method indicated that the IPF method is highly effective at minimizing over-prediction even for multiple simultaneous earthquakes within a short distance, since it adopts a trigger-data classification using velocity amplitude and hypocenter determinations using not-yet-arrived data. The simulation results of the PLUM method demonstrated that the PLUM method is capable of issuing warnings for destructive inland earthquakes more rapidly than the current system owing to the use of additional seismometers that can only be incorporated by this method.

Keywords: Earthquake early warning, 2016 Kumamoto earthquake, Integrated particle filter method, Propagation of local undamped motion method

Introduction

The 2016 Kumamoto earthquake (Kumamoto earthquake sequence) consists of the collective earthquake activity that has continuously occurred in Kumamoto Prefecture and its surrounding areas in Japan since April 14, 2016, at 21:26 (JST) (e.g., JMA 2016). This activity has caused damages in the form of building collapses and landslides and has taken a toll of 49 lives as of June 16, 2016 (Cabinet Office, Government of Japan 2016). The Japan Meteorological Agency (JMA) reported that JMA seismic intensities of 7, which is the maximum on the JMA scale (JMA 1996), were observed during the M6.5 and M7.3 earthquakes that occurred on April 14 and 16, respectively (JMA 2016). This observation marked the first occurrence of a seismic intensity of 7 since the 2011

*Correspondence: kodera@mri-jma.go.jp
[1] Meteorological Research Institute, Japan Meteorological Agency, Tsukuba, Ibaraki, Japan
Full list of author information is available at the end of the article

Springer Open

© The Author(s) 2016. This article is distributed under the terms of the Creative Commons Attribution 4.0 International License (http://creativecommons.org/licenses/by/4.0/), which permits unrestricted use, distribution, and reproduction in any medium, provided you give appropriate credit to the original author(s) and the source, provide a link to the Creative Commons license, and indicate if changes were made.

off the Pacific coast of Tohoku earthquake (Tohoku-oki earthquake) (M9.0). JMA also announced that the number of felt earthquakes reached 1093 in the Kumamoto earthquake sequence from April 14 to 30 (JMA 2016). One of the most notable characteristics of this sequence was a large number of seismic events, including destructive earthquakes, that occurred within a short time across a wide area (Fig. 1a, b). The first earthquake occurred in Kumamoto Prefecture on April 14 at 21:26 with a magnitude of 6.5 and generated many aftershocks within a radius of approximately 10 km from the epicenter. On April 16 at 01:25, a M7.3 earthquake occurred near the epicenter of the first earthquake, causing extremely high seismicity within an approximately 120-km range across Kumamoto and Oita Prefectures.

The earthquake early warning (EEW) system operated by JMA for the general public since 2007 (Hoshiba et al. 2008) issued several "warnings" for the Kumamoto earthquake sequence. The JMA EEW system disseminates a warning for the general public in an effort to mitigate damage from incoming strong motion. Figure 1c shows the number of warnings issued for the Kumamoto earthquake sequence from April 14 to 30. The second and ninth highest daily numbers of warning issuances since 2007 were recorded on April on 16 and 14, respectively. During the Kumamoto earthquake sequence, the system continued to operate under some of the heaviest loading conditions yet observed. An investigation of the system performance under such severe conditions can provide valuable insight into the effectiveness of the method adopted by the current system.

JMA has recently begun developing new techniques to further improve its system performance. JMA plans to introduce the integrated particle filter (IPF) method (Tamaribuchi et al. 2014) to address over-predictions caused by hypocenter mislocation that results from multiple simultaneous earthquake events. The propagation of local undamped motion (PLUM) method is also scheduled to be implemented in order to minimize under-predictions for massive earthquakes with large rupture zones (Kodera et al. 2014). It would be advantageous to analyze actual improvements achievable by these methods for the Kumamoto earthquake sequence because the spatial and temporal patterns of these earthquake occurrences significantly differ from those of past earthquakes.

In this study, we investigated the current system performance for the Kumamoto earthquake sequence, focusing on the cases where warnings were issued or where strong shaking was actually observed. In addition, we performed simulations using the IPF and PLUM methods for characteristic events and evaluated their effectiveness for the Kumamoto earthquake sequence.

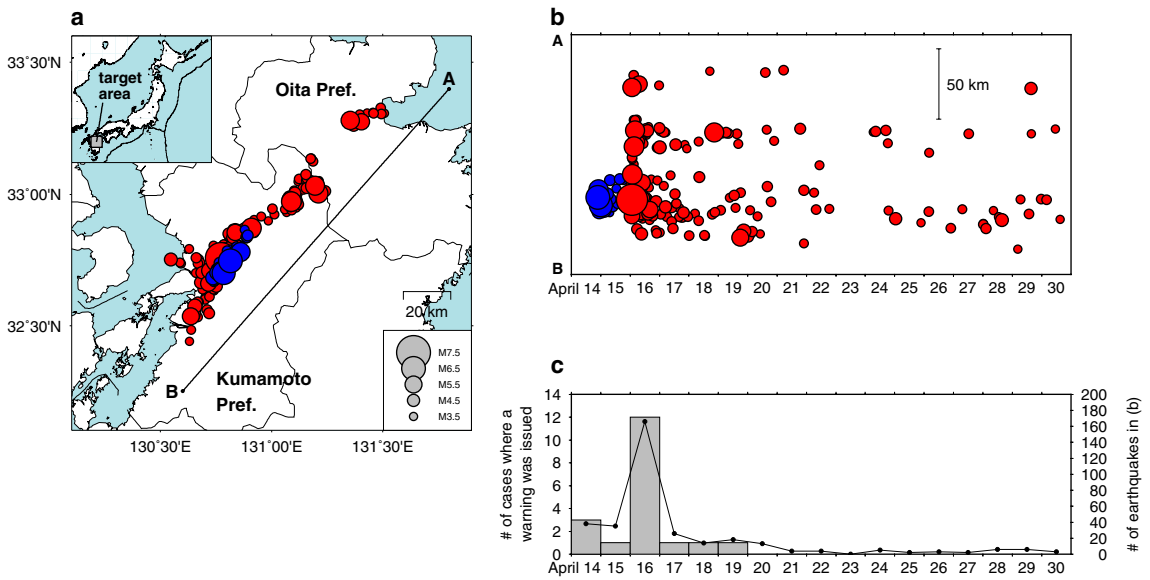

Fig. 1 Spatiotemporal patterns of seismic activity in the Kumamoto earthquake sequence (modified from JMA 2016) and the number of cases where the JMA EEW system issued a warning. **a** Epicenter distribution of the Kumamoto earthquake sequence from April 14 to 30 ($M \geq 3.5$). *Blue circles* indicate earthquakes that occurred before April 16 at 01:25. *Red circles* represent earthquakes that occurred on or after April 16 at 01:25. **b** Detailed spatiotemporal distribution for the rectangular area *A–B* in (**a**). A definition of the *symbols* is the same as in (**a**). **c** Histogram of the daily number of cases where the system issued a warning for the Kumamoto earthquake sequence. A *black line* indicates the number of earthquakes shown in (**b**)

Analysis of the current JMA EEW system performance for the Kumamoto earthquake sequence

The current JMA EEW system predicts seismic intensities on the JMA scale based on hypocenter and magnitude estimations (e.g., Hoshiba 2014). The JMA seismic intensity is represented on a 10-level scale ranging from 0 to 7, where 5 and 6 each contain "upper" (5U and 6U) and "lower" (5L and 6L) subdivisions (JMA 1996). A rough comparison of the JMA scale with the modified Mercalli intensity scale is shown in Fig. 2a. The system is operated mainly on the basis of JMA's strong-motion seismometer network of approximately 270 seismometers deployed at approximately 60-km intervals (Fig. 2b) throughout Japan. The system determines hypocenter locations and magnitudes using trigger data from these strong-motion seismometers. The system also uses approximately 800 high-sensitivity seismometers in Hi-net of the National Research Institute for Earth Science and Disaster Prevention (NIED) (Okada et al. 2004) (see Fig. 2b). The system receives hypocenters estimated by Hi-net stations when the hypocenters are precisely determined. The system issues a warning when (1) the maximum predicted seismic intensity reaches ≥5L and (2-a) the system receives trigger data from at least two strong-motion seismometers or (2-b) the system receives trigger data from at least one strong-motion seismometer and a hypocenter estimated by Hi-net stations. In many cases, the time of warning issuance depends on the time of (1) and (2-a) since receiving hypocenters precisely estimated by Hi-net stations generally requires a relatively long time. A warning is issued according to a predefined area division that consists of 188 areas in total across Japan (Fig. 2c). The initial warning area is defined as areas in which a seismic intensity of ≥4 is predicted at the time. The warning is updated when a seismic intensity of ≥5L is newly predicted for at least one area outside of the most recent warning area. The new warning area additionally incorporates areas with a current predicted seismic intensity of ≥4.

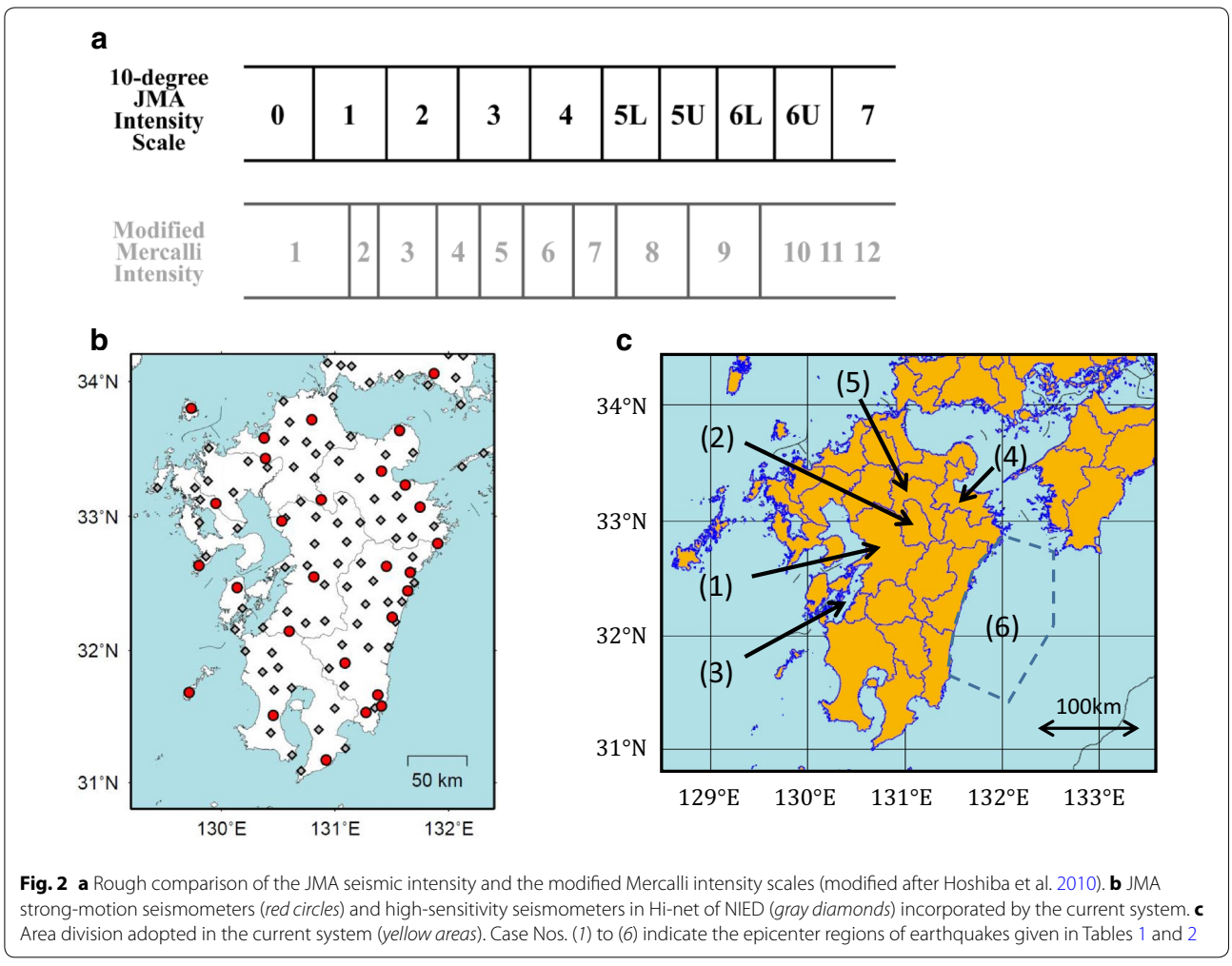

Fig. 2 **a** Rough comparison of the JMA seismic intensity and the modified Mercalli intensity scales (modified after Hoshiba et al. 2010). **b** JMA strong-motion seismometers (*red circles*) and high-sensitivity seismometers in Hi-net of NIED (*gray diamonds*) incorporated by the current system. **c** Area division adopted in the current system (*yellow areas*). Case Nos. (*1*) to (*6*) indicate the epicenter regions of earthquakes given in Tables 1 and 2

From April 14 to 19, the system issued warnings in 19 cases. For these cases, we calculated (1) prediction scores at the time of warning issuance to determine whether a warning was issued based on an accurate prediction result and (2) lapse times from the detection at the first triggered station to verify whether the system processed the observed data without delays. In addition, we investigated four cases in which seismic intensities of ≥5L were actually observed but no warning was issued, to determine whether the system missed or under-predicted strong motion.

The prediction score is defined as the proportion of areas in which the seismic intensity is predicted within a one-level error on the JMA scale among areas where the observed or predicted seismic intensity is ≥4. For instance, if areas A, B, and C have observed seismic intensities of 3, 4, and 5L, and the predicted seismic intensities are 5L (two-level error), 4 (no error), and 4 (one-level error), respectively, the prediction score is 66.7%. Since the system mainly targets large seismic intensities capable of causing serious damage, areas in which both the observed and predicted seismic intensities are less than 4 are excluded from the calculation.

Result 1: cases with a warning issued

We calculated prediction scores and lapse times for each of the 19 warning cases (Table 1) and compared them to the maximum observed seismic intensities (Fig. 3). Twelve out of 19 cases had prediction scores of ≥85%, and the number with scores of <10% was 4 out of 19 (Fig. 3a). Among the cases with a maximum observed intensity of ≥5L, 12 out of 14 had scores of ≥85% and 0 out of 14 had scores of <10%. The number of cases with lapse times of ≤10.0 s and ≤5.3 s was 16 and 12 out of 19, respectively (Fig. 3b). Except for the cases with prediction scores of <10% and maximum seismic intensities of <4, the number of cases with lapse times of ≤10.0 s and ≤5.3 s was 13 and 11 out of 14, respectively.

For the M6.5 earthquake (No. 1 in Table 1), the system issued a warning with a prediction score of 100.0% at 3.8 s after detection (Fig. 4a). The location error of the estimated epicenter was less than 10 km, and the estimated magnitude was equal to the actual magnitude. The warning area covered all the areas where the maximum observed seismic intensity was ≥4 (Fig. 4c). The blind zone was a circular area with a 25-km radius. In the final prediction result by the system, the estimated hypocenter and magnitude were also nearly identical to the actual source parameters (Fig. 4b).

For the M7.3 earthquake (No. 5 in Table 1), the system issued a warning with a prediction score of 45.7% at 3.9 s after detection (Fig. 5a-1) and updated the warning with a prediction score of 97.4% at 8.6 s (Fig. 5a-2). At 3.9 s, the epicenter location was estimated with an error of less than 10 km and the estimated magnitude was 5.9. Although the magnitude was under-estimated, it was large enough to meet the criteria for a warning issuance. The first warning area covered the areas in which seismic intensities of ≥5U were observed (Fig. 5c). The blind zone of the first warning was 26 km. At 8.6 s, the estimated magnitude rose to 6.9 and the predicted seismic intensities at the time satisfied the warning update condition. The second warning area covered all the areas with seismic intensities of ≥5L and most areas with seismic intensities of 4. In the final prediction result, the system estimated a seismic intensity of 7 (Fig. 5b). Note that a M5.7 earthquake occurred at 32.3 s after the M7.3 earthquake, approximately 80 km away (see Fig. 5a-1) (JMA 2016). This M5.7 event did not influence the hypocenter and magnitude estimations for the M7.3 earthquake; however, the system under-predicted a seismic intensity in the area of the M5.7 earthquake. The predicted seismic intensity for the area was 4, based on the estimate for the M7.3 earthquake. The observed seismic intensity was 6L, dominantly generated by strong motion from the M5.7 earthquake (Aoi 2016).

Cases with prediction scores of <10% occurred due to the misclassification of trigger data derived from multiple simultaneous earthquakes. For example, in case No. 14, a M2.9 earthquake occurred at 11:29:00.3 in Kumamoto Prefecture and a M3.2 earthquake occurred at 11:28:57.5 in Oita Prefecture. The system predicted a seismic intensity of 7, estimating an offshore hypocenter with M6.9 (Fig. 6a). However, the maximum observed seismic intensity was just 3 (Fig. 6b). The classification algorithm based on arrival time in the system classified the trigger data from the M2.9 and M3.2 earthquakes into a single event because most stations were triggered by the M2.9 or M3.2 earthquake within 10 s of each other.

There were several cases in which the system issued a warning with a relatively low prediction score (between 10 and 85%) or required a relatively long lapse time (>10 s) for large earthquakes with an observed seismic intensity of ≥5L. In case No. 9, the prediction score was below 85% due to a minor error in the estimated epicenter location. In case No. 11, the prediction score was low at 22.2% because strong motion was localized such that the ground motion prediction equation did not fit the observed seismic intensity distribution. In case No. 2, the system issued a warning for the M5.8 earthquake at 21.2 s after detection. This was due to a lack of data from all the stations within an approximately 90-km radius from the epicenter. These stations were not triggered by the M5.8 earthquake because a M4.6 earthquake occurred in nearly the same location approximately 44 s before the M5.8 earthquake.

Table 1 Warnings from April 14 to 19 and corresponding data from the actual earthquakes

Warning								Actual earthquake		
#	Day	Issuance time	Lapse time/s	Epicenter location	Mag.	Max. seismic intensity	Score (%)	Epicenter location	Mag.	Max. seismic intensity
1	14	21:26:42.5	3.8	(1)	6.5	6U	100.0	(1)	6.5	7
2		22:08:11.9	21.2	(1)	5.4	5L	88.9	(1)	5.8	6L
3		22:38:51.8	5.0	(1)	5.1	5L	100.0	(1)	5.0	5L
4	15	00:03:53.9	4.1	(1)	5.9	5U	91.7	(1)	6.4	6U
5	16	01:25:14.0	3.9	(1)	5.9	5U	45.7	(1)	7.3	7
		01:25:18.7	8.6	(1)	6.9	6U	97.4	(4)	5.7	
6		01:44:17.8	5.2	(1)	5.4	5L	100.0	(1)	5.4	5L
7		01:46:10.7	9.7	(1)	6.0	6L	100.0	(1)	5.9	6L
8		03:03:21.0	5.3	(2)	5.8	5U	100.0	(2)	5.9	5U
9		03:56:02.3	3.4	(2)	5.9	5L	68.4	(2)	5.8	6U
10		04:15:18.9	6.8	(1)	6.4	5U	4.0	(1)	3.5	3
								(2)	3.1	
								(4)	3.8	
11		07:11:43.5	4.3	(4)	5.7	5L	22.2	(4)	5.4	5L
12		07:42:42.8	16.3	(5)	5.7	5L	8.3	(1)	4.2	4
								(2)?	NA	
13		09:48:43.8	5.1	(1)	5.4	5L	85.7	(1)	5.4	6L
14		11:29:08.8	9.5	(6)	6.9	7	2.8	(1)	2.9	3
								(4)	3.2	
15		14:27:10.7	3.9	(2)	5.4	5L	33.3	(1)	4.6	4
16		16:02:10.0	5.1	(1)	5.4	5L	100.0	(1)	5.4	5L
17	17	19:31:17.1	43.9	(1)	5.5	5U	0.0	(4)	2.7	2
								(1)	2.6	
18	18	20:42:07.9	3.9	(2)	5.7	5U	90.9	(2)	5.8	5U
19	19	17:52:23.7	8.2	(1)	5.2	5L	100.0	(1)	5.5	5U

This table lists prediction results with issuance times, prediction scores, and lapse times for issued warnings (the "Warning" section) and information on the actual earthquakes that occurred at the time (the "Actual earthquake" section). In the "Warning" section, a case with more than one row indicates that a warning was updated at least once. A case with more than one row in the "Actual earthquake" section indicates that more than one earthquake occurred simultaneously. The epicenter locations are specified by the numbers shown in Fig. 2c. For case No. 12, the epicenter location and magnitude of the second earthquake have not been precisely determined (the location is roughly estimated to be (2) but is still under investigation). The table is based on the earthquake catalog as of May 2016

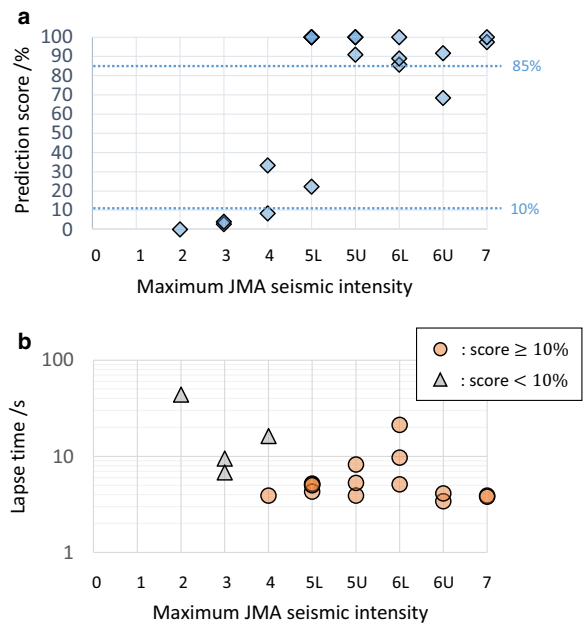

Fig. 3 **a** Comparison of prediction scores with maximum observed seismic intensities. The prediction score at the time of the initial warning issuance for case No. 5 in Table 1 is excluded. **b** Comparison of lapse times with maximum observed seismic intensities. *Orange circles* and *gray triangles* correspond to warnings with prediction scores of ≥10 and <10%, respectively. The lapse time for the second warning issuance for case No. 5 in Table 1 is excluded

Result 2: cases with an actually observed seismic intensity of ≥5L but no warning issued

From April 14 to 30, 18 earthquakes generated a seismic intensity of ≥5L (JMA 2016), equal to the threshold of seismic intensity for warning issuance. The system did not issue warnings for four out of the 18 earthquakes.

Table 2 lists information about the four earthquakes and their corresponding final prediction results. In each case, the system detected the earthquake occurrences and provided source parameter estimations, but warnings were not issued. This was because the predicted maximum seismic intensities did not reach 5L, rather than because the system completely missed the earthquakes.

In case Nos. 1–3, the system provided accurate hypocenter and magnitude estimations, although no warning was issued. The system did not satisfy the warning criteria owing to minor errors in the estimates. In case No. 4, the system under-predicted the maximum seismic intensity by a three-level error because the M4.5 earthquake generated very localized strong motion that was difficult for the system to detect. The maximum observed seismic intensity of 5U was recorded only at the station directly above the epicenter, while the seismic intensities at other stations were ≤3.

Discussion

Results 1 and 2 indicate that the system exhibited remarkable performance, especially for destructive earthquakes where a warning issuance was particularly desirable. According to result 1, the prediction scores were ≥85% in 12 out of the 14 cases in which the observed seismic intensity was ≥5L, and the lapse times were ≤5.3 s in 11 out of the 14 cases. This suggests that, for most of the large earthquakes, the system issued warnings with high accuracy and without lengthy delays. According to result 2, in the four cases where no warnings were issued, the system estimated accurate source parameters (Nos. 1–3) or predicted appropriate ground shaking except for the event where strong motion was very localized (No. 4). This indicates that the system did not miss or seriously under-predict strong motions for any large earthquake from April 14 to 30.

On the other hand, result 1 also reveals that the system has difficulty distinguishing between earthquakes that occur within a short distance and time of one another. Since the Tohoku-oki earthquake, JMA has continued to improve its algorithm for classifying trigger data (e.g., JMA 2012), which has allowed the system to distinguish multiple simultaneous earthquakes within a few hundred kilometers more robustly. However, in the Kumamoto earthquake sequence, several earthquakes occurred simultaneously within a very narrow range, which was difficult even for the improved system to effectively process. Some earthquakes simultaneously occurred within distances comparable to the spatial interval of the seismometer network. A trigger-data classification based only on arrival time differences appears to pose a fundamental obstacle for separating trigger data from multiple earthquakes within such short distances.

Although the system was required to process considerable earthquake data in a short period, it operated stably and successfully issued warnings for destructive inland earthquakes of the Kumamoto earthquake sequence. This implies that the method adopted by the current system will work effectively for similar destructive inland earthquakes that may occur in the future. At the same time, if the system continues to implement the current method, the trigger-data classification algorithm will need to be fundamentally improved.

Performance analysis of new techniques: simulations of IPF and PLUM methods

We evaluated the performance of two new techniques, the IPF and PLUM methods, for the Kumamoto earthquake sequence and simulated their prediction behavior for characteristic events.

The IPF method is a hypocenter estimation algorithm that uses a Bayesian estimation framework and a particle filter technique (Tamaribuchi et al. 2014; Liu and Yamada

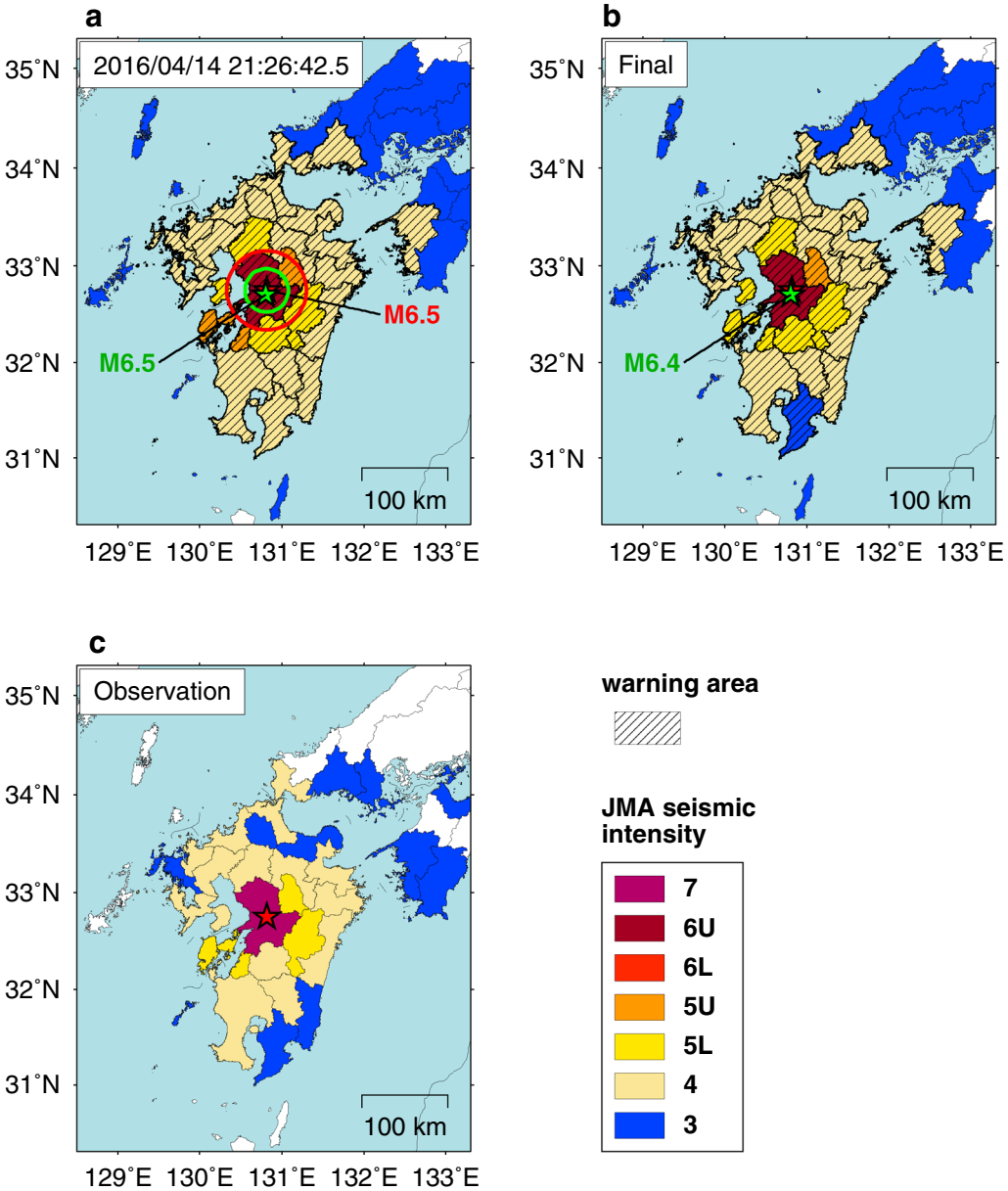

Fig. 4 **a** Warning area and prediction result for the warning issuance by the current system for case No. 1 in Table 1. *Colors of each area* indicate the predicted JMA seismic intensities at the time, with the warning area marked by *shading*. The actual and estimated epicenters are indicated by *red* and *green stars*, respectively, with corresponding magnitudes in the *same colors*. A *red line* represents the theoretical P-wave, and a *green line* indicates the theoretical S-wave. The time at the *upper left* corresponds to the warning issuance time. **b** Final prediction result by the current system for case No. 1. Definitions of *colors*, *shading*, and *symbols* are the same as in (**a**). **c** Actual seismic intensities observed in case No. 1. *Colors of each area* indicate the observed JMA seismic intensities. A *red star* marks the actual epicenter

2014). The IPF method uses many types of observed data in addition to arrival time, such as velocity amplitude, not-yet-arrived data (Horiuchi et al. 2005), and B–Δ (Odaka et al. 2003; Tsukada et al. 2004), in its trigger-data classification and hypocenter determination. The IPF method is expected to distinguish and separately process multiple simultaneous earthquakes more robustly than the current method, which relies only on arrival time.

The PLUM method is a simple wavefield estimation algorithm derived from Hoshiba's (2013) method, which does not require source parameter determination (Kodera et al. 2014). The PLUM method calculates

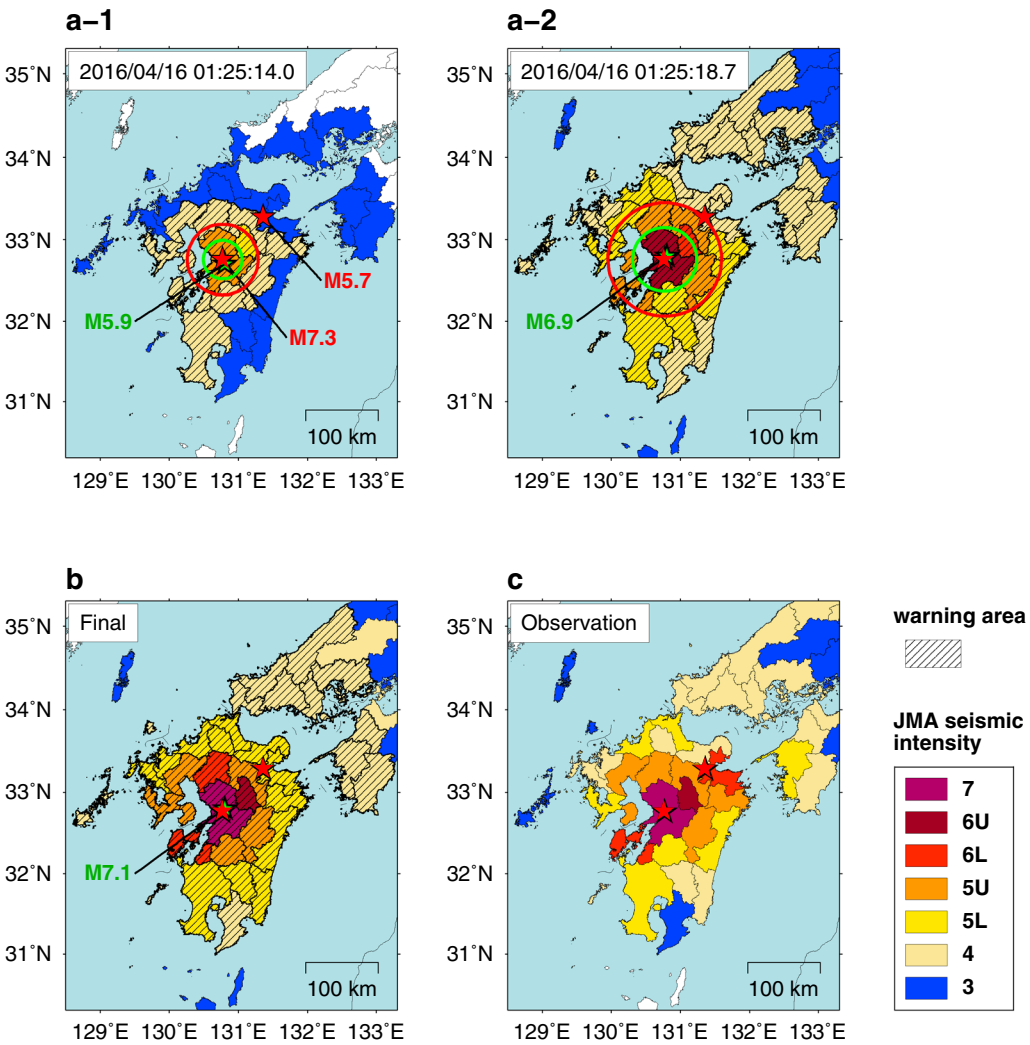

Fig. 5 **a-1**, **2** Warning areas and prediction results for the initial (**a-1**) and second (**a-2**) warning issuances by the current system for case No. 5 in Table 1. **b** Final prediction result by the current system for case No. 5. **c** Actual seismic intensities observed in case No. 5. Definitions of *colors*, *shading*, and *symbols* are the same as in Fig. 4

predicted seismic intensities based on the following equation.

$$Ir_{\mathrm{pred}} = \max(Ir_1, Ir_2, \ldots, Ir_n), \tag{1}$$

where Ir_{pred} is the predicted seismic intensity of a target point and $Ir_i (i = 1, 2, \ldots, n)$ indicates real-time seismic intensities (Kunugi et al. 2013) observed at stations located within a distance of 30 km from the target point. Note that site amplification factors are taken into account in the actual calculation. The PLUM method is expected to stably estimate strong motion generated by very large earthquakes with wide rupture zones and is suited to the rapid detection of inland earthquakes. The PLUM method can operate with a denser seismic network than that used by the current and IPF methods since it requires only observed real-time seismic intensities, which are available even from stations with a lower S/N ratio than the level required by the current and IPF methods. JMA plans to use approximately 400 additional strong-motion seismometers for the PLUM method (Fig. 7) in future operations.

We selected six cases for the simulations: Case Nos. 1 and 5 given in Table 1 were chosen to evaluate prediction accuracy and warning issuance rapidity for destructive inland earthquakes and case Nos. 10, 12, 14, and 17 were chosen to examine behaviors in multiple simultaneous earthquakes that could lead to over-prediction. The IPF method was carried out with the same trigger data

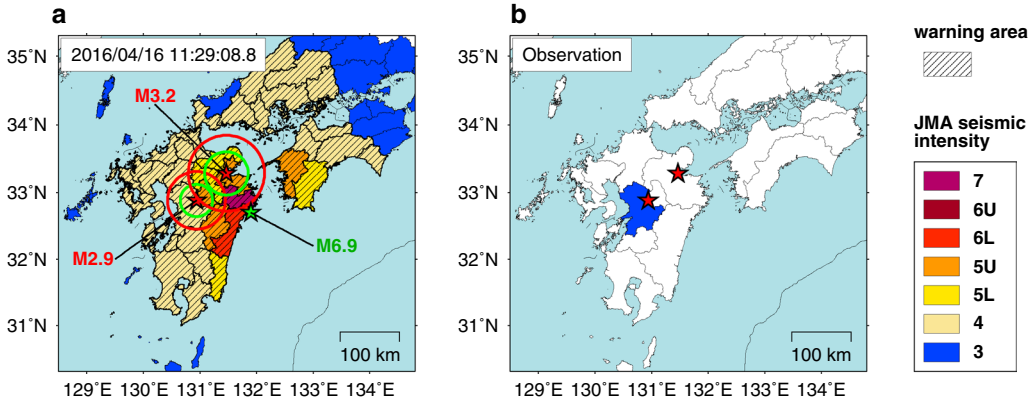

Fig. 6 **a** Warning area and prediction result for the warning issuance by the current system for case No. 14 in Table 1. **b** Actual seismic intensities observed in case No. 14. Definitions of *colors*, *shading*, and *symbols* are the same as in Fig. 4

Table 2 Major earthquakes with no warning issued and the corresponding final prediction results

Actual earthquake						Final prediction result			
#	Day	Origin time	Epicenter location	Mag.	Max. seismic intensity	Epicenter location	Mag.	Max. seismic intensity	Score (%)
1	15	01:53:01.4	(1)	4.8	5L	(1)	4.8	4	100.0
2	16	07:23:54.3	(1)	4.8	5L	(1)	4.6	4	100.0
3	19	20:47:03.3	(1)	5.0	5L	(3)	4.8	4	100.0
4	29	15:09:34.3	(4)	4.5	5U	(4)	4.1	3	0.0

This table lists the four cases from April 14 to 30 in which seismic intensities of ≥5L were actually observed but warnings were not issued by the system. The definitions of the epicenter locations are the same as in Table 1

from strong-motion stations that the current system actually received and processed. The IPF method did not use high-sensitivity seismometers in Hi-net. For the PLUM method, a dataset was created by calculating real-time seismic intensities from waveforms recorded during the events by the existing and additional strong-motion seismometers (approximately 670 points in total across Japan). The time window of the real-time seismic intensity was set to 5 s. In the PLUM method simulations, calculations were done at 1-s intervals and delays related to computation and data transmission were not taken into account.

Results

We calculated the prediction scores and warning issuance times for each of the six cases (Table 3). For case Nos. 1 and 5, warnings were issued in both the IPF and PLUM method simulations. The initial issuance times for the IPF method were 0.4 s later in case No. 1 and 0.8 s later in No. 5 than those in the current method. Those for the PLUM method were 1.5–2.5 s faster in case No. 1 and 3.0–4.0 s faster in No. 5. Note that the issuance times for the PLUM method have an uncertainty of 1 s since the PLUM method was performed using 1-s intervals in the simulations. The prediction scores of the IPF method were comparable to those of the current method in case No. 1 and slightly lower in No. 5. For the PLUM method, prediction scores were lower in both case Nos. 1 and 5. For case Nos. 10, 12, 14, and 17, which the current method over-predicted, the IPF method issued no warnings except for case No. 10. The PLUM method issued no warnings for any case.

Figure 8 shows the warning areas and predicted seismic intensities in the IPF and PLUM methods for case No. 1. The IPF method estimated an accurate hypocenter and magnitude when issuing a warning (Fig. 8a-1). The IPF method issued a warning for nearly the same areas as the current method (see Fig. 4a), with a blind zone of 26 km. In the final prediction result, the maximum predicted seismic intensity rose from 5U to 6U (Fig. 8a-2), and the prediction score reached 100.0%. In the PLUM method, a warning was initially issued for the areas closest to the epicenter (Fig. 8b-1). The blind zone at the initial issuance was 15–19 km. Eight seconds later, the PLUM method updated the warning and the surrounding areas were included in the warning area (Fig. 8b-2). Although the

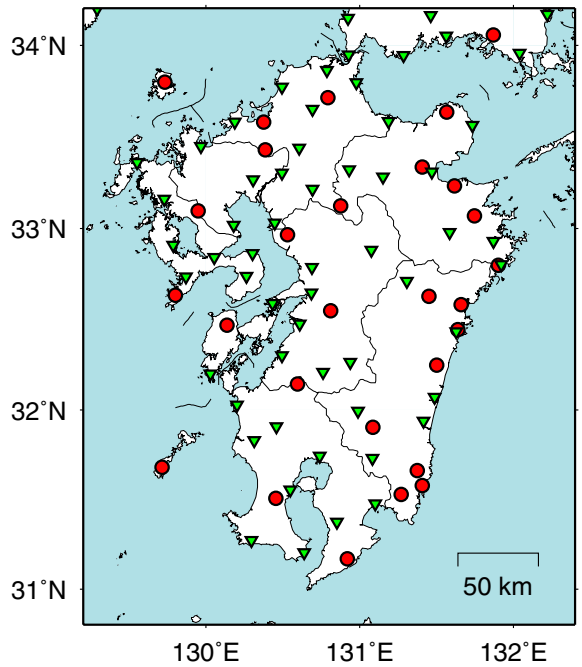

Fig. 7 Distribution of additional stations planed by JMA for use with the PLUM method (*green inverted triangles*) and the existing strong-motion seismometers (*red circles*)

second (and final) warning area was much smaller than those in the current and IPF methods, it covered all areas with an observed seismic intensity of ≥5L (see Fig. 4c). In the final prediction result, the prediction score of the PLUM method was 95.2%. The PLUM method over-predicted a seismic intensity for the area to the southwest of the epicenter with a two-level error due to a mismatch in strong-motion attenuation (Fig. 8b-3).

Figure 9 illustrates the warning areas and predicted seismic intensities in the IPF and PLUM methods for case No. 5. When the IPF method issued a warning, the estimated hypocenter was located very close to the correct position; however, the estimated magnitude was 2.0 units lower than the actual magnitude (Fig. 9a-1). The blind zone was 29 km. All areas with an observed seismic intensity of ≥5L were included in the warning area (see Fig. 5c), although the warning area in the IPF method was smaller than the final warning area in the current method (see Fig. 5a-2). The estimated magnitude rose to 7.0 in the final prediction result, but the warning was not updated because a seismic intensity of ≥5L was not predicted outside of the warning area (Fig. 9a-2). The final prediction score was 97.4%. The IPF method under-predicted the seismic intensity in the area of the M5.7 earthquake, as did the current method. In the PLUM method, a warning was initially issued for the areas closest to the epicenter (Fig. 9b-1). The blind zone was 9–14 km, which was much smaller than those in the current and IPF methods. The warning was later updated four times, as S-wave propagation continued (Fig. 9b-2–5). The final warning area in the PLUM method was similar to that in the IPF method and covered all areas, except one, with a seismic intensity of ≥5L. In the final prediction result (Fig. 9b-6), the PLUM method predicted a seismic intensity of 7. Additionally, the strong motion generated by the M5.7 earthquake was also predicted. On the other hand, the mismatch in strong-motion attenuation resulted in over-prediction for several areas around the epicenters.

For cases involving multiple simultaneous earthquakes (Nos. 10, 12, 14, and 17), over-predicted warnings were not issued, except in the IPF method simulation for case No. 10. In case Nos. 12 and 17, the IPF method did not

Table 3 Warning results for the current, IPF, and PLUM methods for the six selected cases

# in Table 1	Current method		IPF method		PLUM method	
	Issuance time	Score (%)	Issuance time	Score (%)	Issuance time	Score (%)
1	21:26:42.5	100.0	21:26:42.9	96.0	21:26:40.0–41.0	5.3
					21:26:48.0–49.0	36.8
5	01:25:14.0	45.7	01:25:14.8	65.7	01:25:10.0–11.0	0.0
					01:25:16.0–17.0	8.6
	01:25:18.7	97.4			01:25:23.0–24.0	34.3
					01:25:31.0–32.0	45.7
					01:25:34.0–35.0	48.6
10	04:15:18.9	4.0	04:15:19.6	7.1	(no issued warning)	
12	07:42:42.8	8.3	(no issued warning)		(no issued warning)	
14	11:29:08.8	2.8	(no issued warning)		(no issued warning)	
17	19:31:17.1	0.0	(no issued warning)		(no issued warning)	

This table lists issuance times and prediction scores for warnings in case Nos. 1, 5, 10, 12, 14, and 17 in Table 1. Cases with multiple rows indicate that warnings were updated once or more. Issuance times for the PLUM method were obtained with 1-s accuracy since calculations were performed at 1-s intervals

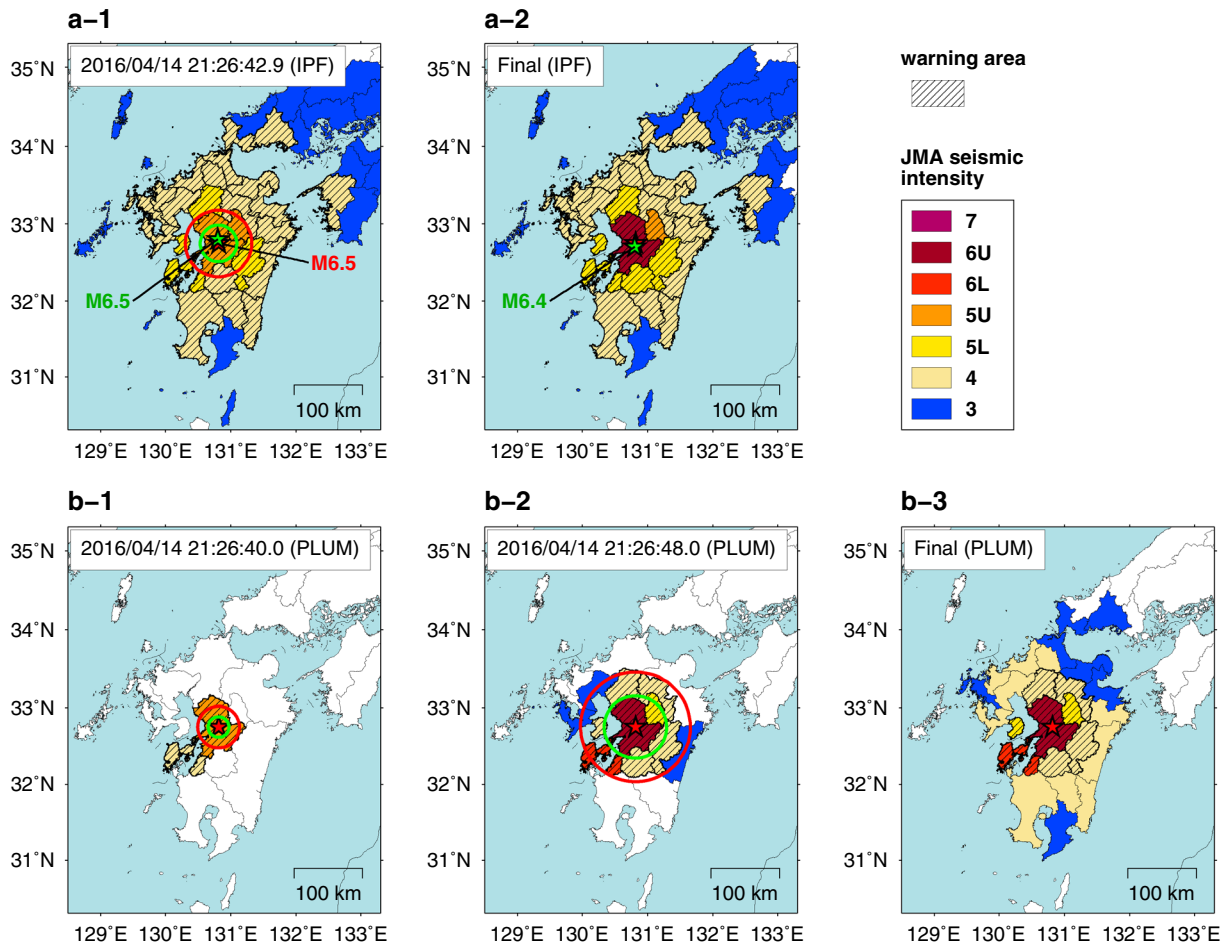

Fig. 8 **a-1** Warning area and prediction result for the warning issuance by the IPF method for case No. 1. **a-2** Final prediction result by the IPF method for case No. 1. **b-1**, **2** Warning areas and prediction results at the initial (**b-1**) and second (**b-2**) warning issuances by the PLUM method for case No. 1. The issuance times are considered to be the lower limits in this figure. **b-3** Final prediction result by the PLUM method for case No. 1. Definitions of *colors*, *shading*, and *symbols* are the same as in Fig. 4

generate over-predictions and correctly isolated and individually processed trigger data from the multiple simultaneous earthquakes. This successful isolation resulted from the use of observed velocity amplitudes in classifying trigger data. In case Nos. 10 and 14, the IPF method failed to distinguish the trigger data because the earthquakes had very similar origin times and magnitudes; however, the IPF method reduced over-prediction effects relative to the current method. The hypocenter location estimates in the IPF method were closer to the actual locations than those in the current method, owing to the use of not-yet-arrived data in hypocenter determination. In case No. 10, the IPF method estimated a hypocenter located close to the station that observed the maximum displacement amplitude and calculated a magnitude of 5.8, which was 0.6 units lower than that in the current method. Although the IPF method ended up issuing an over-predicted warning, the number of warning areas was roughly half of that in the current method. In case No. 14, the IPF method estimated a hypocenter close to the M3.2 earthquake and the estimation result did not satisfy the warning criteria. In the PLUM method, no warning was issued for any of the cases because large real-time seismic intensities were not observed.

Discussion

The simulation results for case Nos. 1 and 5 indicate that the IPF method performs as well as the current method for destructive inland earthquakes. The IPF method successfully issued warnings for all areas affected by strong motion within a delay of <1 s, compared to the current method. The prediction score at the time of the warning issuance in case No. 5 was lower than that in the current method; however, the warning area was large enough to

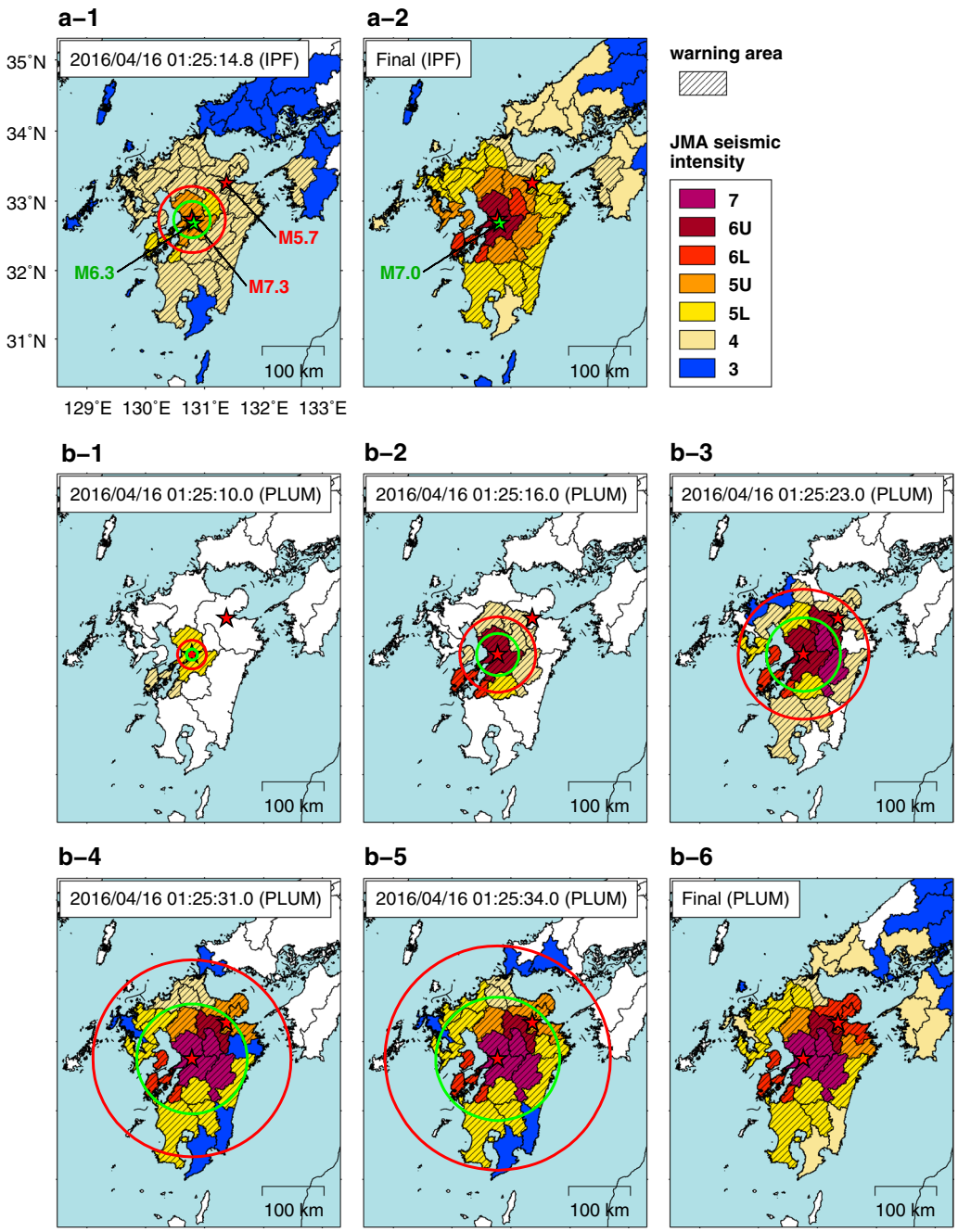

Fig. 9 **a-1** Warning area and prediction result for the warning issuance by the IPF method for case No. 5. **a-2** Final prediction result by the IPF method for case No. 5. **b-1–5** Warning areas and prediction results for the initial to fifth warning issuances by the PLUM method for case No. 5. The issuance times are considered to be the lower limits in this figure. **b-6** Final prediction result by the PLUM method for case No. 5. Definitions of *colors*, *shading*, and *symbols* are the same as in Fig. 4

sufficiently cover all the areas struck by strong motion. The slight delays in warning issuance arose from a difference in the time of magnitude estimation, which can be improved by increasing the frequency of magnitude calculation.

The simulation results also reveal that the PLUM method is superior in initial warning issuance compared to the current method. In the PLUM method, the initial warning issuance times were 1.5–2.5 s ahead of those in the current method in case No. 1 and 3.0–4.0 s in No. 5, which shrank the blind zones by 7–11 km in No. 1 and 15–20 km in No. 5. These rapid issuances resulted from the use of a denser seismic network. The first and second

stations that detected the strong motion were among the additional seismometers incorporated only in the PLUM method. The PLUM method seems to be effective at providing longer lead times for areas closest to an epicenter, where the strongest shaking is likely to be observed.

On the other hand, the PLUM method did not provide long lead times for the surrounding areas. According to the simulations for case Nos. 1 and 5, the warning areas of the PLUM method did not include the surrounding areas until the S-waves approached these areas. For the surrounding areas, the IPF method provides longer lead times than the PLUM method. The combined use of the IPF and PLUM methods would be more effective at maximizing the total lead times for all the areas, as mentioned by Kodera et al. (2014).

Note that the PLUM method detected and predicted the strong motion produced by the M5.7 event in case No. 5. Prediction methods based on source parameter estimates would be unable to predict such strong motion, or even recognize such earthquake occurrence, because the waveform of the M5.7 event overlapped completely with that of the M7.3 event, and the STA/LTA trigger related to the M5.7 event did not function. This indicates that the PLUM method and other wavefield estimation approaches are needed for robust strong-motion prediction for intense seismic activities.

Both the IPF and PLUM methods exhibited better performance for the multiple simultaneous earthquakes that resulted in over-predicted warnings in the current method. In the IPF method, the classification algorithm using the observed velocity amplitude improved its ability to discriminate between earthquake occurrences. In addition, hypocenter determinations using not-yet-arrived data enhanced the robustness of the source parameter estimates when the classification of trigger data was partially incorrect. Introducing many types of data other than arrival time seems to be a promising approach for minimizing over-predictions related to source parameter estimation. In the PLUM method, small multiple simultaneous earthquakes pose no serious problems since such earthquakes only generate small real-time seismic intensities not targeted by the PLUM method, which implies that the PLUM method is sufficiently robust for multiple simultaneous earthquakes.

Further enhancements in the performance of the IPF and PLUM methods appear to be possible by incorporating more observational facilities into the system. According to the PLUM method simulations, the size of the blind zone strongly depends on the density of the incorporated seismic network. The size of a blind zone would be further reduced if real-time seismic intensities are available from a denser seismic network (e.g., a low-cost sensor network). The PLUM method may have less difficulty incorporating low-cost sensors since the algorithm it uses is very simple and requires only real-time seismic intensities. In the IPF method, a denser seismic network may further improve the ability of trigger-data discrimination, enabling the IPF method to recognize the spatial distribution of velocity amplitude with a higher resolution.

The IPF and PLUM method simulations indicate that these new methods are superior to the current method and that introducing these methods would further improve the performance of the JMA EEW system for the Kumamoto earthquake sequence, although the current method itself exhibited excellent performance. To more effectively mitigate damage from impending destructive inland earthquakes in the future, the IPF and PLUM methods should be implemented and operated in the actual system.

Conclusions

We evaluated the current JMA EEW system performance for cases with warnings issued from April 14 to 19 and those in which a seismic intensity of $\geq$5L was actually observed but no warning was issued from April 14 to 30. The analysis of cases with warnings revealed that the system issued warnings with high accuracy and without lengthy delays for most of the large earthquakes in the Kumamoto earthquake sequence. Among the 14 cases where the observed seismic intensity was $\geq$5L, warnings with a prediction score of $\geq$85% were issued in 12 cases and those with a lapse time of $\leq$5.3 s were issued in 11 cases. The analysis of the cases in which no warning was issued demonstrated that the system did not miss or seriously under-predict strong motion for any large earthquake from April 14 to 30. These results indicate that the method adopted by the current system has the ability to operate stably and successfully issue warnings for destructive inland earthquakes even under conditions of extremely heavy loading. On the other hand, the analysis of cases with warnings also reveals that the current system has difficulties in separating trigger data from multiple earthquakes occurring within short distances and times. There were four cases of warnings with a prediction accuracy of <10%, which resulted from hypocenter mislocations due to incorrect classification of trigger data from multiple simultaneous earthquakes.

We simulated the behavior of the IPF and PLUM methods for the M6.5 and M7.3 earthquakes and for multiple simultaneous earthquakes that produced over-predicted warnings in the current system. The IPF method exhibited high performance for the M6.5 and M7.3 earthquakes, as did the current method. For multiple simultaneous earthquakes, the IPF method did not issue over-predicted warnings in 3 out of the 4 cases. The

PLUM method initially issued warnings 1.5–2.5 s earlier than the current method for the M6.5 earthquake and 3.0–4.0 s earlier for the M7.3 earthquake, due to the use of a denser seismic network. The PLUM method did not result in over-predictions for the multiple simultaneous earthquakes because large real-time seismic intensities were not observed. These results indicate that the IPF and PLUM methods are superior to the current method and that implementing these methods in the actual system would lead to further improvements in the system performance and more effective damage mitigation of impending destructive inland earthquakes in the future.

Abbreviations

JMA: Japan Meteorological Agency; EEW: earthquake early warning; IPF: integrated particle filter; PLUM: propagation of local undamped motion; NIED: National Research Institute for Earth Science and Disaster Prevention.

Authors' contributions

YK designed the study, conducted the analysis, simulated the PLUM method, and drafted the manuscript. JS, NH, SA, MM, and YN participated in operation of the JMA EEW system, maintaining the database related to the system, and simulating the IPF method. MH helped interpret the results and draft the manuscript. All authors read and approved the final manuscript.

Author details

[1] Meteorological Research Institute, Japan Meteorological Agency, Tsukuba, Ibaraki, Japan. [2] Seismology and Volcanology Department, Japan Meteorological Agency, Chiyoda-ku, Tokyo, Japan.

Acknowledgements

We would like to thank Dr. Adrien Oth, an anonymous reviewer, and Dr. Takuya Nishimura (editor) for their valuable comments on the manuscript. Koji Tamaribuchi helped us interpret the simulation results of the IPF method. The JMA EEW system is based on a joint research between JMA and the Railway Technical Research Institute and technological achievements by NIED. The JMA EEW system is operated using seismic data from observational facilities of NIED in addition to those of JMA. Seismic intensity and waveform data were obtained from the JMA network, K-NET of NIED, and local governments and municipalities. The earthquake catalog was compiled by JMA and the Ministry of Education, Culture, Sports, Science and Technology on the basis of seismic waveforms provided by NIED, Hokkaido University, Hirosaki University, Tohoku University, the University of Tokyo, Nagoya University, Kyoto University, Kochi University, Kyushu University, Kagoshima University, the National Institute of Advanced Industrial Science and Technology, the Geospatial Information Authority of Japan, the Japan Agency for Marine-Earth Science and Technology, Aomori Prefectural Government, Tokyo Metropolitan Government, Shizuoka Prefecture, the Hot Springs Research Institute of Kanagawa Prefecture, and JMA. Most of the figures were drawn using the Generic Mapping Tools (Wessel and Smith 1998). This work was partially supported by JSPS KAKENHI Grant Number JP25282114.

Competing interests

The authors declare that they have no competing interests.

Received: 13 July 2016 Accepted: 15 November 2016
Published online: 01 December 2016

References

Aoi S (2016) The Kumamoto earthquake sequence from the perspective of observed seismic data. http://www.bosai.go.jp/event/2016/pdf/20160424_aoi.pdf. Accessed 29 June 2016 (**in Japanese**)

Cabinet Office, Government of Japan (2016) On prompt information such as damage situations related to the earthquake located in Kumamoto-ken Kumamoto-chiho in 2016 (as of June 16, 2016 at 17:15). http://www.bousai.go.jp/updates/h280414jishin/pdf/h280414jishin_31.pdf. Accessed 29 June 2016 (**in Japanese**)

Horiuchi S, Negishi H, Abe K, Kamimura A, Fujinawa Y (2005) An automatic processing system for broadcasting earthquake alarms. Bull Seismol Soc Am 95:708–718. doi:10.1785/0120030133

Hoshiba M (2013) Real-time prediction of ground motion by Kirchhoff–Fresnel boundary integral equation method: extended front detection method for earthquake early warning. J Geophys Res 118:1038–1050. doi:10.1002/jgrb.50119

Hoshiba M (2014) Review of the nationwide earthquake early warning in Japan during its first five years. In: Shroder JF, Wyss M (eds) Earthquake hazard, risk, and disasters. Elsevier, Amsterdam. doi:10.1016/B978-0-12-394848-9.00019-5

Hoshiba M, Kamigaichi O, Saito M, Tsukada S, Hamada N (2008) Earthquake early warning starts nationwide in Japan. EOS Trans AGU 89:73–74. doi:10.1029/2008EO080001

Hoshiba M, Ohtake K, Iwakiri K, Aketagawa T, Nakamura H, Yamamoto S (2010) How precisely can we anticipate seismic intensities? A study of uncertainty of anticipated seismic intensities for the earthquake early warning method in Japan. Earth Planets Space 62:611–620. doi:10.5047/eps.2010.07.013

Japan Meteorological Agency (1996) Seismic intensity. Gyosei, Tokyo (in Japanese)

Japan Meteorological Agency (2012) The forth technical panel in the committee of evaluation and improvement of the earthquake early warning (document No. 1). http://www.data.jma.go.jp/svd/eqev/data/study-panel/eew-hyoka/t04/20121001_siryou1.pdf. Accessed 29 June 2016 (**in Japanese**)

Japan Meteorological Agency (2016) On the 2016 Kumamoto earthquake (the 39th report) (press release). http://www.jma.go.jp/jma/press/1606/10a/kaisetsu201606101000.pdf. Accessed 29 June 2016 (**in Japanese**)

Kodera Y, Yamada Y, Hirano K, Morimoto M, Hoshiba M, Nakamura M (2014) Earthquake early warning system combined with real-time ground motion prediction (Japan Geoscience Union Meeting 2014). https://confit.atlas.jp/guide/event-img/jpgu2014/SSS28-02/public/pdf?type=in. Accessed 29 June 2016

Kunugi T, Aoi S, Nakamura H, Suzuki W, Morikawa N, Fujiwara H (2013) An improved approximating filter for real-time calculation of seismic intensity. Zisin 2(60):223–230. doi:10.4294/zisin.65.223 **(in Japanese with English abstract and figure captions)**

Liu A, Yamada M (2014) Bayesian approach for identification of multiple events in an early warning system. Bull Seismol Soc Am 104:1111–1121. doi:10.1785/0120130208

Odaka T, Ashiya K, Tsukada S, Sato S, Ohtake K, Nozaka D (2003) A new method of quickly estimating epicentral distance and magnitude from a single seismic record. Bull Seismol Soc Am 93:526–532. doi:10.1785/0120020008

Okada Y, Kasahara K, Hori S, Obara K, Sekiguchi S, Fujiwara H, Yamamoto A (2004) Recent progress of seismic observation networks in Japan—Hi-net, F-net, K-NET and KiK-net. Earth Planets Space 56:xv–xxviii. doi:10.1186/BF03353076

Tamaribuchi K, Yamada M, Wu S (2014) A new approach to identify multiple concurrent events for improvement of earthquake early warning. Zisin 2(67):41–55. doi:10.4294/zisin.67.41 **(in Japanese with English abstract and figure captions)**

Tsukada S, Odaka T, Ashiya K, Ohtake K, Nozaka D (2004) Analysis of the envelope waveform of the initial part of P-waves and its application to quickly estimating the epicentral distance and magnitude. Zisin 2(56):351–361 **(in Japanese with English abstract and figure captions)**

Wessel P, Smith WHF (1998) New, improved version of generic mapping tools released. EOS Trans AGU 79:579. doi:10.1029/98EO00426